Regression rate Measurements in Lab-Scale Hybrid Burners

P. Tadini, C. Paravan, F. Maggi, M. Boiocchi, G. Colombo and L.T. DeLuca.
Space Propulsion Laboratory
Aerospace Science & Technology Dept., Politecnico di Milano
Via La Masa 34, 20156 Milan, Italy

Abstract

As an answer to the need for precise regression rate (r_f) characterization in hybrid rockets, the Space Propulsion Laboratory (SPLab) of Politecnico di Milano is working on the implementation of original techniques and sensors. Three of them are here presented. A non-intrusive, optical time-resolved technique for the r_f in 2D-radial burner is discussed first. Then, an optical-fiber system for the data reduction of a slab rocket is discussed. Finally, an intrusive technique, based on wire-cut sensor embedded in the solid fuel is described. Advantages and disadvantages of each technique are underlined.

Nomenclature

Latin Symbols

a_D	:	multiplier factor in Eq. (1), mm / s^{n_D}
a_r	:	multiplier factor in Eq. (10), $mm/(s\ G_{ox}^{n_r})$
C_s	:	specific heat of the solid phase, *J/kg K*
D	:	diameter, *mm*
D_0	:	nominal initial diameter, *mm*
$\overline{D}$	:	space-averaged diameter, *mm*
$\overline{D}_{ign}$	:	space-averaged diameter at strand ignition, *mm*
$\overline{D}_i$	:	i-th sampled space-averaged diameter, *mm*
G_{ox}	:	oxidizer mass flux, *kg/(m²s)*
$< G_{ox} >$	:	time-averaged oxidizer mass flux in Eq. (9), $kg/(m^2 s)$
h^*	:	Convective heat transfer coefficient $W/(m^2\ K)$
L_p	:	grain length, *mm*
$\dot{m}_f$	:	fuel mass flow rate, *g/s*
$\dot{m}_{ox}$	:	oxidizer mass flow rate, *g/s*
n_D	:	time exponent in Eq. (1)
n_r	:	time exponent in Eq. (10)
O / F	:	Oxidizer to Fuel ratio
r_f	:	regression rate, *mm/s*
$< r_f >$	:	time-averaged regression rate, *mm/s*
$\bar{r}_{f_{i+\frac{1}{2}}}$	:	TOT regression rate, *mm/s*
R^2	:	correlation index
t	:	time, *s*
t_0	:	reference time in Eq. (1), *s*
T_{ign}	:	ignition temperature, *K*
t_{ign}	:	ignition time, *s*
T_{fl}	:	flame temperature, *K*
t_{fin}	:	final time, *s*
$T_{s,in}$	:	initial solid fuel surface temperature, *K*
$T_{s,film}$	:	film solid fuel surface temperature, *K*
$T_{s,fin}$	:	final solid fuel surface temperature, *K*

Greek Symbols

ρ_f	:	solid fuel density, g/cm^3
κ_c	:	thermal diffusivity, m^2/s

: **Abbreviations**

2D	:	two-dimensional
fps	:	frames per second
GOX	:	Gaseous OXygen
HTPB	:	Hydroxyl-Terminated Polybutadiene
TOT	:	Thickness Over Time

1. Introduction

Nowadays, a great effort in propulsion research field is focused on hybrid rocket engines, as valuable options for several applications, such as orbital transfers, space debris removal [1], suborbital flights and private access to space [2]. Hybrid propulsion mediates benefits and drawbacks from both liquid and solid rocket technology. On one side, it enables throttleability and re-ignition typical of liquids, specific impulse levels which fall in between the performance of solid and liquid propulsion systems, and a higher mean propellant density due to the use of a solid fuel. Moreover, intrinsic safety, possibility of non-toxic propellant use and low cost features are favorable characteristics that increase the interest in the development of these systems. A hybrid rocket engine typically features the oxidizer in the liquid or gaseous state, while the fuel is in the solid state. Low regression rates and poor combustion efficiencies are the main drawbacks of these systems. In addition, scaling effects are fairly predictable. Considering the regression rate, different techniques have been investigated for its enhancement, spanning from the use of advanced additives to different means for oxidizer injection providing vortex combustion [3][4]. The solid fuel regression rate is the most important parameter used to describe hybrid rocket internal ballistics. In the field of experimental research, the accurate determination of this parameter is essential for the comprehension the combustion phenomena. Several techniques have been developed for this purpose, resorting to those used for the ballistic investigation of solid rocket motors [5]. Intrusive and non-intrusive techniques can be identified.

For intrusive techniques, sensors are embedded within the solid fuel grain, providing the desired measurement by interpretation of physical transducer variations. Typically, this kind of sensors are made by electric resistances and thermocouples, but even capacitance sensors are applied [6] [7] [8]. A resistance-based sensor for direct regression rate measurement was proposed by Monti and Mazzola [7]. In this study the possibility of tracking regressing surface in time by electric resistance changes of a conductive material shaped as burning strand head-end was considered. Electric resistance methods offer possible advantages as good accuracy and low cost. Similarly (but with a lower accuracy) regression rate can be evaluated by thermocouples embedded in the solid fuel grain. In this case the approach is quite similar to the typical fuse-wire method used for solid rocket motors [5], but with the possible advantage of the solid fuel grain temperature profile characterization [9].

A simple and widespread technique for time-averaged regression rate determination is non-intrusive, and is based on solid fuel mass (or thickness) measurement before and after combustion [10] [11]. This technique is subjected to low accuracy and possible ambiguous determination of the burning duration. Experimental methods able to provide more detailed information are preferable [6]. In particular, ultrasound technique supplies an accurate measurement of the local, instantaneous regression rate, though possible limitations can derive from the coupling with the tested fuel (e.g. ultrasound absorption). Space-averaged and instantaneous combustion monitoring can be achieved by evaluation of the Helmholtz mode frequency [12], whereas X-ray radiography performed at Pennsylvania State University is probably the most accurate technique available. The latter enables instantaneous regression rate measurement over the entire solid fuel grain length [13][14], but the hardware has high operating costs.

The Space Propulsion Laboratory (SPLab) is developing advanced proprietary sensors and post-processing techniques for the ballistic characterization of solid fuels burning in quasi-steady and forced transient conditions.

The development activities exploit three different hybrid burners currently on service at the SPLab: an optical, non-intrusive technique is applied in a 2D-radial setup, an optical-fiber sensor is under testing in a 2D-slab combustion chamber, while a swirl injector enables cross-comparison between the optical technique and an intrusive wire-cut sensor.

2. Non-Intrusive Technique: Optical Time Resolved

An optical, time-resolved technique for regression rate data reduction was implemented at the SPLab. The method was developed and improved using a 2D-radial micro burner, whose schematic overview is shown in Figure 1. The combustion chamber is a stainless steel cylinder housing the injector head and optical accesses for test visualization. The main parameter of interest is the regression rate of the single perforation cylindrical solid fuel sample. During combustion, the burning cross-section of the tested fuel is fully visible thanks to a proper combination of lateral windows and a 45 degree mirror placed inside the combustion chamber.

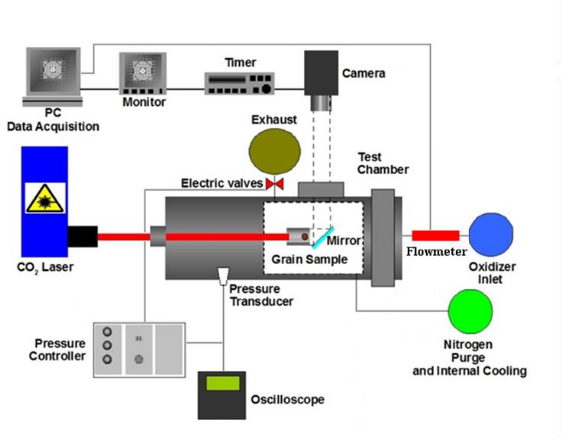

Figure 1- 2D-radial micro burner scheme

Both oxidizer mass flow and chamber pressure of the test rig can be regulated independently, thus allowing different test conditions to be easily explored. The oxidizer is fed by cylinders and is injected through 8 holes realized in the internal surface of the sample holder, thus providing control on the nature of the flow investing the fuel sample. Both axial and swirled oxidizer flowing over the tested fuel surface can be achieved. The oxidizer flow is measured by a mass flow-meter and regulated by a needle valve. A secondary feed line enables a Nitrogen flow to cool the chamber walls and prevent soot deposition hindering the burning process visualization. A dump pipeline connecting the combustion chamber to servo-valves grants a controlled pressure level during combustion [15]. Sample ignition is achieved by a pyrotechnic primer charge, inserted in the central port of the solid fuel grain and in turn ignited by a CO_2 laser beam impinging on it. The overall combustion process is recorded by a range of video-cameras operated at different speeds, from 25 up to 1000 fps, depending on the expected fuel regression rate. The video signal, after passing through a timing device, is digitalized by a computer where all raw data are collected and stored.

2.1 Operator-Based Post-Processing

The SPLab optical time-resolved technique is based on strand central port diameter sampling from the recorded combustion video. Diameter sampling starts after primer charge ignition, once the head-end central port diameter becomes visible. Data sampling extends till the end of the combustion (depending on visualization quality). During the combustion, central port diameter is sampled along different radial directions, depending on combustion uniformity. At least two directions are considered (usually vertical and horizontal), performing three different measurements each. The sampled space-averaged local diameters are evaluated considering brightness/contrast differences between the flame zone and the regressing surface. Diameter sampling frequencies in the range 1-10 Hz are achieved, depending on local grain head-end visualization quality [16]. Flame-flickering and head-end burning influence the local diameter measurements at higher frequencies [16][17][18]. The $\overline{D}_i$ is defined as the mean diameter resulting by averaging the different space-averaged local diameters. The $\overline{D}_i$ sequence is a discrete information in time. By the power-law fitting presented in Eq. (1) the discrete $\overline{D}_i$ originates a continuous $\overline{D}(t)$

$$\overline{D}(t) - D_0 = a_D \cdot (t - t_0)^{n_D} \ , \ t \geq t_{ign} > t_0 \ . \tag{1}$$

The $\overline{D}(t) - D_0$ is defined starting from t_{ign}. The latter is ad-hoc defined as the one maximizing the data fitting of Eq. (1). The achieved t_{ign} can be compared to the corresponding ignition delay estimated under the hypothesis of exclusive convective heating [19] as

$$t_{ign,conv} = \frac{\pi}{4} \cdot \kappa_c \cdot \left[\frac{\rho_f \cdot C_s \cdot (T_{s,in} - T_{s,fin})}{h^* (T_{fl} - T_{s,film})} \right]^2 \tag{2}$$

The denominator of Eq. (2) provides an estimation of the convective heat transfer from the flame to the solid fuel grain during the ignition transient. In order to account for the changes of surface temperature during heating, a surface film temperature is considered in the calculations. The $T_{s,film}$ is defined as the average value resulting from the initial and final solid fuel grain temperatures (298 K and 820 K respectively [3]). The convective heat transfer coefficient, h^*, is determined by the Gnielinski formula [20]. A detailed comparison of t_{ign} vs. $t_{ign,conv}$ showing their agreement under the investigated conditions is reported in [15][17][18][21].

The diameter evolution in time defined by the simple Eq. (1) captures the monotonic behavior of $\overline{D}(t)$ observed in quasi-steady operating conditions. Moreover, due to Eq. (1) smooth behavior, possible data scattering that would affect a TOT-based approach are avoided. Starting from Eq. (2), the time-resolved ballistics of the burning strand can be defined according to

$$r_f\left(t \geq t_{ign}\right) = \frac{1}{2}\frac{d\left[\overline{D}(t) - D_0\right]}{dt} = \frac{1}{2}a_D n_D (t - t_0)^{n_D - 1} \tag{3}$$

$$G_{ox}(t \geq t_{ign}) = \frac{\dot{m}_{ox}(t)}{\pi \frac{\overline{D}(t)^2}{4}} = \frac{\dot{m}_{ox}(t)}{\pi \frac{\left[D_0 + a_D (t - t_0)^{n_D}\right]^2}{4}} \tag{4}$$

$$\dot{m}_f(t \geq t_{ign}) = \rho_f \ A_f(t) \ r_f(t) = \rho_f \ \pi \ \overline{D}(t) \ L_p \ r_f(t) = \rho_f \ \pi\left[D_0 + a_D (t - t_0)^{n_D}\right] \ L_p \ r_f(t) \tag{5}$$

$$O/F(t \geq t_{ign}) = \frac{\dot{m}_{ox}}{\dot{m}_f} = \frac{\dot{m}_{ox}}{\rho_f \ \pi D \ L_p \ r_f(t)} = \frac{\dot{m}_{ox}}{\rho_f \ \pi \left[D_0 + a_D (t - t_0)^{n_D}\right] \ L_p \ r_f(t)} \tag{6}$$

The instantaneous time-resolved data [Eq. (1), (3)-(6)] can be integrated in time to obtain the time-averaged ballistics. This provides additional information that can be compared to the corresponding TOT data. Thus, the consistency between different data reduction techniques can be assessed according to the following constraints

$$r_f\left(t_{ign}\right) = \frac{1}{2}a_D n_D (t_{ign} - t_0)^{n_D - 1} \overset{?}{=} \frac{n_D}{2} \cdot \frac{\overline{D}(t_{ign}) - D_0}{t_{ign} - t_0} \tag{7}$$

$$< r_f\left(t_{fin}\right) > = \frac{1}{t_{fin} - t_{ign}} \int_{t_{ign}}^{t_{fin}} r_f(t) \cdot dt \overset{?}{=} \frac{1}{2} \cdot \frac{\overline{D}(t_{fin}) - \overline{D}(t_{ign})}{t_{fin} - t_{ign}} \tag{8}$$

$$< G_{ox}\left(t_{fin}\right) > == \frac{1}{t_{fin} - t_{ign}} \int_{t_{ign}}^{t_{fin}} G_{ox}(t) \cdot \ dt \overset{?}{=} \frac{\dot{m}_{ox}}{\frac{\pi}{4} \cdot \left[\frac{\overline{D}(t_{ign}) + \overline{D}(t_{fin})}{2}\right]^2} \tag{9}$$

The time-resolved technique enables a complete ballistic characterization of the considered fuel formulation over a range of G_{ox}. In spite of this, turbulence effects and the diffusive nature of the hybrid flame yield data scattering. Therefore, the different $\overline{D}(t)$ collected for a certain fuel formulation in given operating conditions are collapsed in an ensemble average curve of the kind of Eq. (2) including all of the performed tests. In this way the $r_f\ (G_{ox})$ characterizing the tested fuel can be identified, and a power-law approximation of r_f vs. G_{ox} can be proposed as

$$r_f(G_{ox}) = a_r \cdot G_{ox}(t)^{n_r} \ , \ t \geq t_{ign} > t_0 \tag{10}$$

Ensemble curve enables definition of proper error bars for $\overline{D}(t)$ and $r_f(G_{ox})$, as described in [17]. Time-resolved technique operating steps are hereby presented and discussed for a typical run and ensemble average [HTPB in GOX, with p_c= 10 bar and initial G_{ox} = 380 kg/(m^2 s)]. The $\overline{D}_i$ discrete sequence is reported in Figure 2.

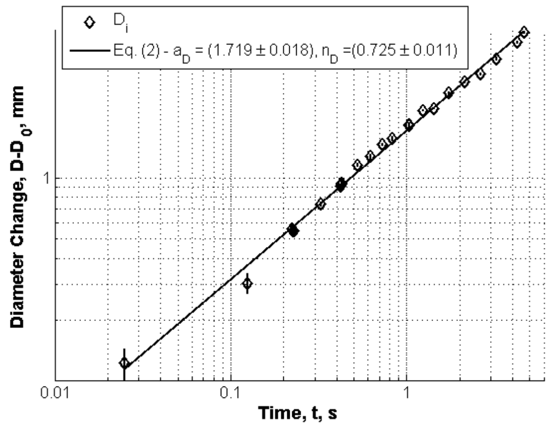

Figure 2: $\overline{D}_i$ and their power-law fitting according to Eq. (2) for Test No. 04, R^2 = 0.99.

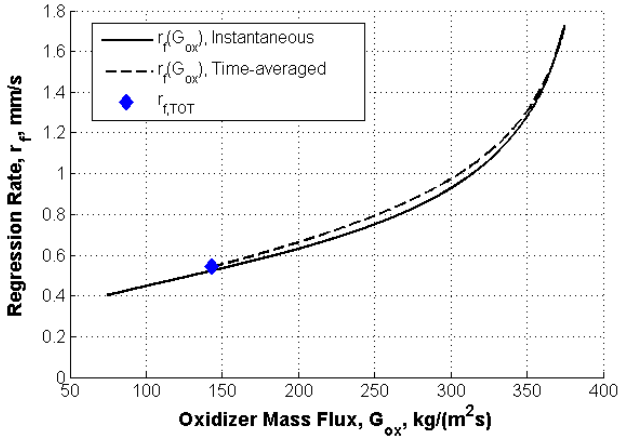

Figure 3: Ballistic characterization of HTPB, Test No. 4. The time-averaged ballistics can be directly related to TOT data, showing the consistency of the achieved results.

Under quasi steady operating conditions, port diameter exhibits a monotonic increase in time, well captured by the proposed approach (see Table 1). Thanks to the ad-hoc definition of t_{ign} data fitting of Eq.(2) is characterized by high R^2 values. As diameter increases in time, G_{ox} decreases (for steady-state $\dot{m}_{ox}$) and so does the convective heat transfer. This, in turn, yields a decreasing r_f behavior for increasing time/decreasing G_{ox}, as observed in Figure 3. Defining the r_f by Eq. (3), an exact time-averaged value can be determined. The $<r_f>$ results in agreement with the corresponding TOT datum evaluated over the entire run duration. The consistency between time-resolved and TOT data is high, as testified by the data presented in Table 1.

Table 1: Power law fitting of $\bar{\boldsymbol{D}}(\boldsymbol{t})$, relevant parameters of Eq.(2) and consistency checks for HTPB/GOX under reference condition.

Test No.	$a_D, mm/s^{n_D}$	n_D	$R^2, Eq.(2)$	$Eq.(5)$ [a]	$Eq.(6)$ [a]	$Eq.(7)$ [a]
01	(1.618 ± 0.022)	(0.763 ± 0.013)	0.99	0.8	-5.2	1.3
02	(1.742 ± 0.012)	(0.724 ± 0.006)	0.99	0.4	-1.0	-2.7
03	(2.120 ± 0.016)	(0.601 ± 0.008)	0.99	-0.1	5.6	-3.4
04	(1.719 ± 0.018)	(0.725 ± 0.011)	0.99	1.8	-0.8	-2.0
05	(1.901 ± 0.028)	(0.632 ± 0.016)	0.98	-0.5	-3.5	3.4
06	(1.660 ± 0.011)	(0.674 ± 0.007)	0.99	0.2	0.6	-0.3
Ensemble	(1.773 ± 0.003)	(0.702 ± 0.002)	0.98	- [b]	- [b]	- [b]

[a] Consistency checks results are expressed as percent values evaluated with respect to the TOT data.

[b] Consistency checks are applied only to single test data.

Collapsing the performed single runs in the ensemble average curve, the result shown in Figure 4 is achieved. The latter shows a $n_r \sim 0.8$, in agreement with diffusion-limited models for the turbulent boundary layer combustion [10]. The data fitting of Eq. (8) to the instantaneous $r_f(G_{ox})$ results relatively low due to the different behavior of the time-resolved data and the power-law approximation [22].

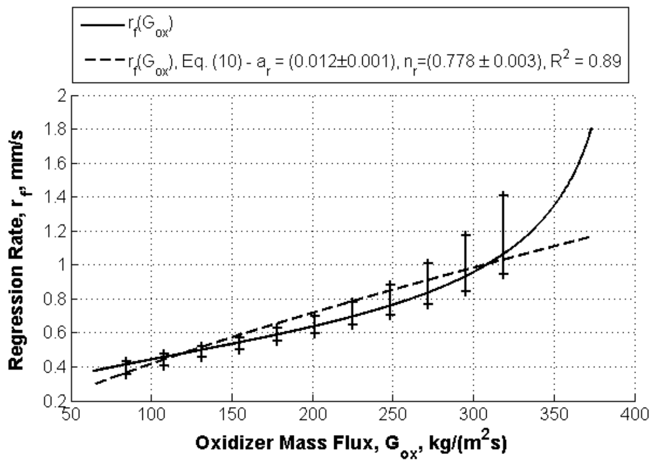

Figure 4: Ballistic characterization of HTPB under reference condition, ensemble average. Details on solid fuel ballistic response are given in [17][18][22].

2.2 Automated Software-Based Post-Processing

As an alternative to the operator-based approach, an automatic post-processing software for the digital image processing of the combustion visualizations was developed. It is based on *OpenCV* Library and compiled in *C++*. This software should enable diameter data sampling at high frequency. This is done by a different approach to diameter measurement. While in the operator-based approach diameters are sampled along different radial directions to determine $\overline{D}(t)$, in this variant of the technique, the whole port boundary is considered.

The post-processing consists of three steps. First of all, each frame of the colored recorded video is filtered to obtain a binary B/W image. The latter contains only the region representing the regression surface. The filtering operation involves:

- *color emphasize*, to increase the difference between light and dark regions;
- *low light filter*, to delete components with low bright level;
- *smoothing*, blur effect to clean the image from no relevant components, not deleted by the previous filtering;
- *saturation*, to obtain the grayscale image underlining high bright regions.

Thus, it is possible to proceed with the frame *binarization*. This attributes a value of 0 or 1 to each pixel, depending on its brightness with respect to the threshold level defined by the user. However, the filtering process does not allow to eliminate completely the recorded image noise, especially that due to the flame oscillation near the port perimeter (see blue circle in Figure 5).

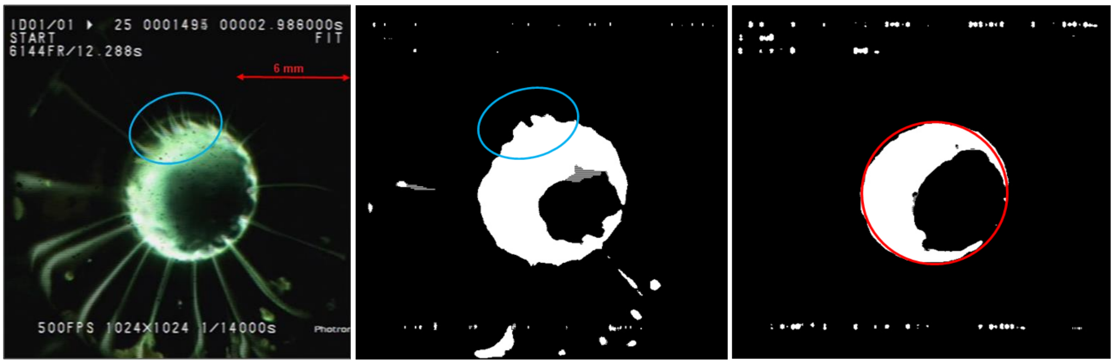

Figure 5: Original image frame (left side), binary frame (center) and post-AND frame with ellipse perimeter interpolation (right side).

A too high filter intensity can significantly reduce the image quality. Hence, the second step, consists in the noise elimination by the application of the *AND logical operator* between consecutive binary frames. This approach is a simple binary product, which allows masking a desired pixel with the corresponding one in the following frame. The noise removal is performed by applying the AND operator to a certain number of binary frames, which depends on the video frame rate (a too high number of frame involved can modify the flame profile). Now the image is ready for the measurement. In the third step, the definition of the flame region boundaries is required. Because of the possible anisotropic combustion (with central port slightly different from a circular shape), an elliptical perimeter is identified for the tracking of the port shape evolution during the run (red ellipse in Figure 5). Nevertheless, despite the image filtering and the AND application, usually still few noise/ high bright regions posted in the dark region exist. This problem is solved considering a *topological filter*, which selects only the interested image region. Finally, in order to increase the ellipse interpolation accuracy, a flame interruption is imposed (preferably where the flame is thinnest).

The output of this software contains the measured ellipse characteristics, from which is possible to evaluate the ellipse eccentricity and the mean port diameter for each frame. By generating the diameter-to-time curve, with a power law interpolation [see Eq. (1)], the instantaneous fuel regression rate can be determined as previously discussed [Eqs. (3)-(6)] with the same procedure described in the previous paragraph. Generally, the number of diameter measures saved for one combustion visualization is between 100 and 500. Thus, the description of the port regression over the combustion time appear well described respect to the low number of measures provided by the operator-based post processing (15-20).

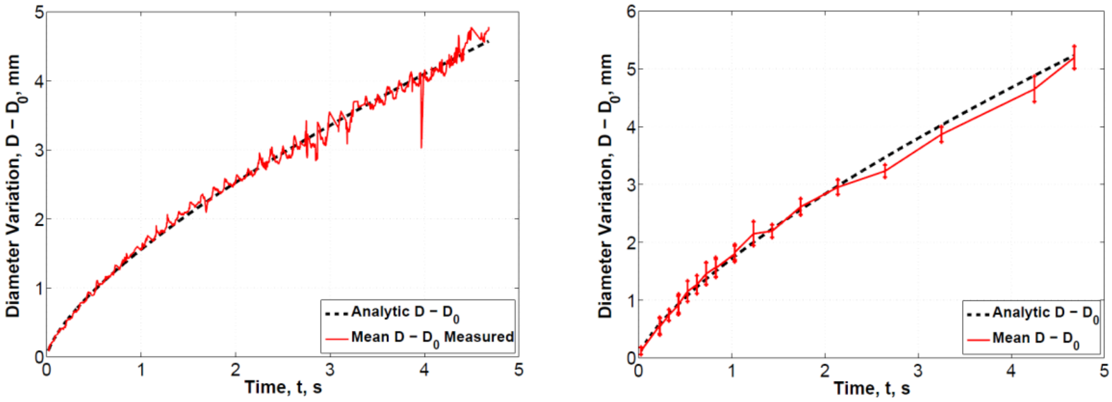

Figure 6: Diameter power law fitting (black) compared with experimental data (red). Automatic-Based (left) vs. Operator-Based (right).

In Figure 6, a comparison between the operator-based and automatic-based approaches is presented. In the automated-port identification procedure, the first diameter measurements are not considered in order to improve the data fitting of Eq. (1). This is due to possible transient phenomena limiting the detection of the port boundaries by the software algorithm. From the comparison reported in Figure 6, the differences in $D\text{-}D_0$ measurement between operator- and software-based approaches are shown. The automatic-based approach seems inclined to a diameter underestimation respect to the operator-based. The difference is probably due to the filtering operation made by the automatic software. In fact, depending on the video quality and flame brightness, it is necessary to tailor the video filtering in order to have a good description of the central port erosion by the created ellipse. On the contrary, the user can directly measure the right boundary which detaches the flame from the fuel surface, evaluating a more precise mean diameter, though this yields to a reduced number of measured diameters. For example, the big pick in Figure 6 (left), after 4 seconds of combustion is due to flame recirculation which it was misinterpreted by the software.

2.3 Results Comparison

Once obtained the $\overline{D}(t) - D_0$ power-law fitting from the video post-processing, the instantaneous regression rate and the power-law approximation of r_f vs. G_{ox} can be evaluated. In Figure 7 one can see the ballistic characterization of Test No. 4, performed with the two different approaches.

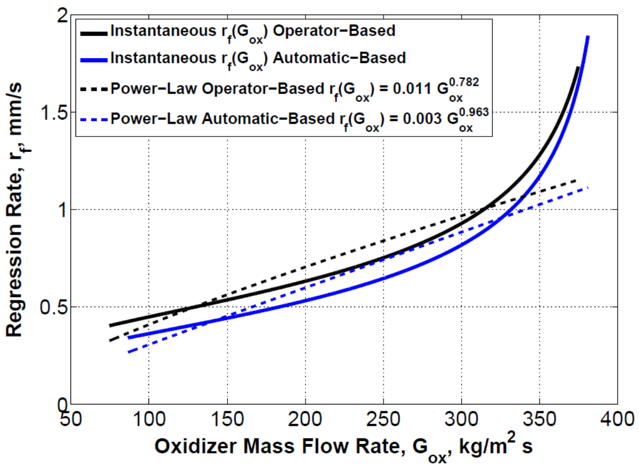

Figure 7: Instantaneous $r_f(G_{ox})$ and Power-law $r_f(G_{ox})$ (dashed line) for Test No. 4. Comparison between operator-based (black) and automatic-based (blue) approaches.

Table 2: Power-law approximation comparison

Parameter	**Operator-Based**	**Automatic-Based**	**Percentage Difference, %**
a_r, *mm m^2/kg*	0.011	0.003	72.7
n_r	0.783	0.963	-22.9

The automatic-based software is able to follow the inner port erosion during the combustion, providing a correct regression rate behavior. However, the difference between the power-law parameters, with respect to the operator-based results, is significant. The exponent n_r is higher for the automatic-based method, because of the steep slope of the instantaneous r_f (blue) at G_{ox} > 360 kg/m^2 s. Also the initial values of the regression rate result higher than the operator-based measure. These dissimilarities are probably due to the software capacity to correctly identify the inner port perimeter during the transient phase after the ignition, where flame stabilization and head-end combustion phenomena are more pronounced.

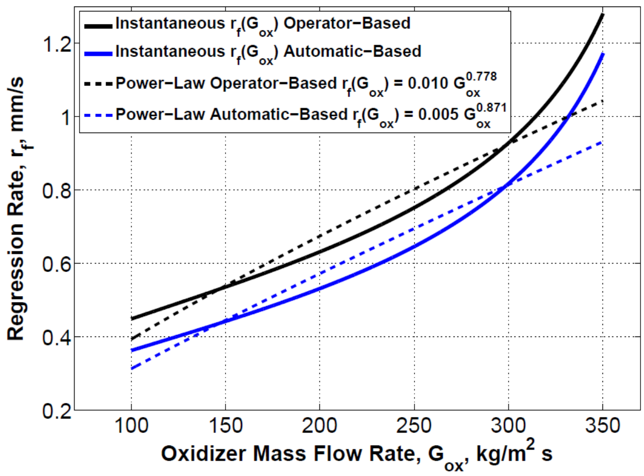

Figure 8: Instantaneous r_f (G_{ox}) and Power-law r_f (G_{ox}) (dashed line) for Test No. 4. Comparison between operator-based (black) and automatic-based (blue) approach over the same G_{ox} interval.

By comparing the regression rate over the same oxidizer mass flux interval [100 kg/ (m^2 s) ≤ G_{ox} ≤ 350 kg/(m^2 s)], one can see, in Figure 8, a quite similar trend for the two considered methods. In this case, the power-law approximation parameters result closer. The automatic-based curves appear shifted down respect to the operator-based. This behavior is due non-optimal video filter settings, for the considered test. During the automatic diameter sampling it was possible to observe that the ellipse perimeter did not overlap perfectly the solid surface boundary, resulting little bit smaller, thus yielding the achieved regression rate effect. Video filter tailoring cannot be easily automated and, at now, the filter levels are heuristically determined

.

In conclusion, the automatic-based software is able to provide a quite good ballistic characterization for test firings in 2D-radial burners, but the measure accuracy is still lower than the operator-based approach. Further development of the algorithm and improvements of the filtering operation are required.

3. Non-Intrusive Technique: Optical Fibers

Fiber-optic sensors represent one of the most innovative techniques [23][24] used to measure very high speed events such as the velocity of detonation inside high explosives. Commercial fiber optics in combination with relatively inexpensive commercial electronic devices can be used to measure the regression rate of hybrid fuels. An experimental set-up was implemented at SPLab and some preliminary firing tests were conducted with a complete non-intrusive apparatus based on a multi-fiber optic sensor.

The free head-end of each optical fiber of the sensor is protected with a ceramic material and leaned to the solid fuel sample inside the combustion chamber. Each optical fiber is connectorised to correctly match with the analyzer. An electronic analyzer consisting in an array of 8 photodiodes (Light Intensity Analyzer 8 channels LIA08) was used to convert a luminous signal flowing through the fiber, into an electrical signal. Finally a plot reporting the trend of the light intensity of eight luminous signals versus time was obtained and used to calculate the value of the regression rate. Each fiber in this experimental configuration could be treated as a luminous switch. When the combustion surface is far from the first fiber, each one are into the dark so all the electrical signals from the photodiodes array are negligible. As the luminous region of the flame is approaching to the fiber optic sensor, thanks to the not perfect opacity of the fuel, more than one fiber could be able to collect and convey photons to the corresponding photodiodes. Fortunately, compared with the light intensity of the flame region, the light diffused below the combustion surface is negligible. Another interesting point is linked with the intrinsic characteristic of the fiber optic: to have an optimal propagation of the light into the fiber, the angle between the light source and the fiber core axis has to be less than a small (critical) angle. Knowing the correct spacing of each fiber and the difference in time between each luminous signal and the other reported on the plot, by a simple linear regression is possible to obtain the regression rate.

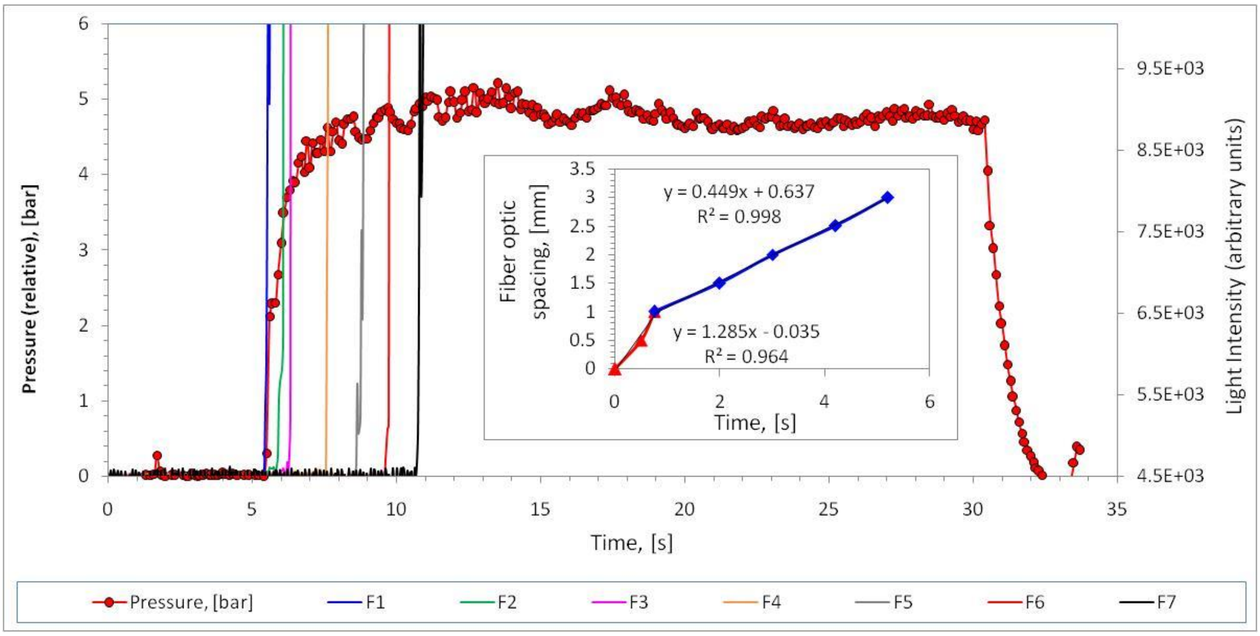

Figure 9: Firing test pressure trace of a HTPB slab fuel. Vertical lines represent luminous signals from fiber optic leaned to the fuel inside the combustion chamber.

Figure 9 shows a typical pressure trace of a firing test of a HTPB sample slab with all the fiber optic signals obtained by LIA08. The plot of the regression shows that during the initial part of the combustion the regression rate is higher than in the later part: the result is a double slope curve. The average combustion rate calculated with an integral method (based on the measure of the sample mass before and after the combustion) gives a value of 0.44 mm/s.

4. Intrusive Technique: Wire-Cut Sensor

SPLab has developed a discrete resistive sensor based on the wire-cut technique, commonly used for characterization tests in solid propellant strand-burners [25]. A set of wires is placed in the propellant strand connected to a resistor, as shown in the electronic scheme of Figure 10. In this array the resistors are connected in parallel each other, and the whole block is connected to a power source by a known resistance (R2, probing resistance). The voltage across the latter is monitored in time.

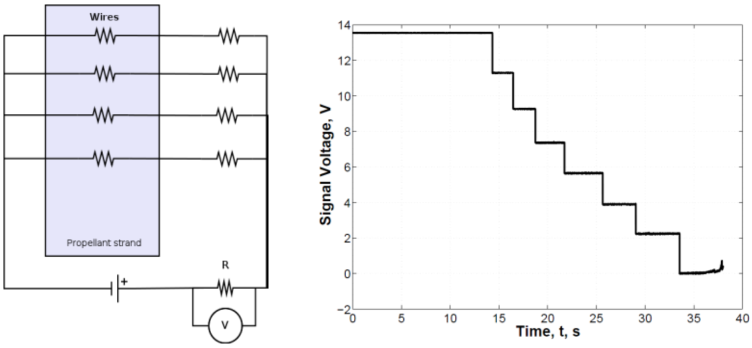

Figure 10: Electronic Scheme (left) and Voltage probe across R2 (right).

As the sample burns, the wires progressively break due to the approaching flame. Thus, the circuit electric resistance varies and this, in turn, changes current and voltage across R2. In the Volt-Time diagram, shown in Figure 10, the measurement takes the shape of a series of steps whose amplitudes can be tuned by adjusting the value of the resistors in the circuit. The SPLab has worked at developing this kind of measurement and at porting it in a configuration that is suitable for in-situ installation inside the fuel grain before the casting.
Sensor development and initial validation were conducted in a lab-scale nozzle-less swirl burner, see Figure 11 (left), specifically designed for the scope. The burner neither is pressurized nor has a gas dynamic nozzle. The injection part contains a finned disk for swirling flow generation, Figure 11 (center).

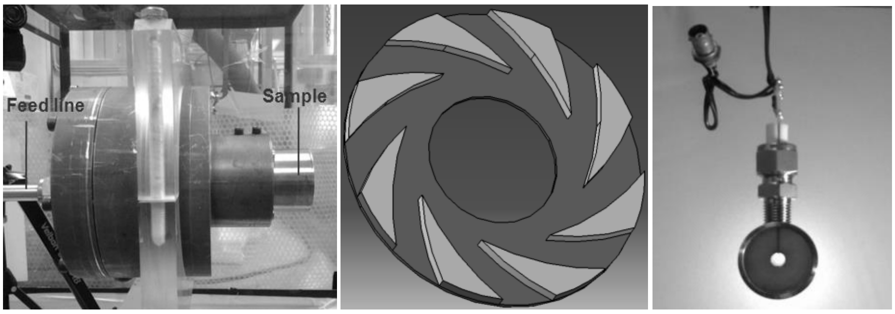

Figure 91: Injector side view (left), swirling finned disk (center), sample with embedded sensor(right).

Considering the Beer and Chigier's convention, based on momentum conservation [25], the geometrical swirl number of the swirler is 4.75. The disk is interchangeable, no-swirl disk without oriented wings is available. The combustion occurs directly into the fuel sample perforation, at atmospheric conditions. The sensor is installed before the fuel casting in the solid fuel grain sample, with a inner port of 6 mm, outer diameter of 30 and length of 70 mm. In Figure 11 (right), one can see the orientation of the sensor inside the solid fuel. The wire-cut voltage signal is read by a oscilloscope. The feed system is composed by two inlets: the first for oxygen, used for combustion, the second for nitrogen, used to interrupt the combustion. Sample ignition is achieved by a small quantity of kerosene-gel deposited in the head-end central port and in turn ignited by a hot wire. The optical acquisition is performed by a high-speed camera which can observe the head-end of the strand, thanks to injector original design.

The sensor validation was performed using HTPB-based (hydroxyl-terminated polybutadiene) fuel grains. In Figure 12 (left), one can see the comparison between the optical and sensor measures of the regression surface, the resulting traces successfully compare to direct observation of the combustion.

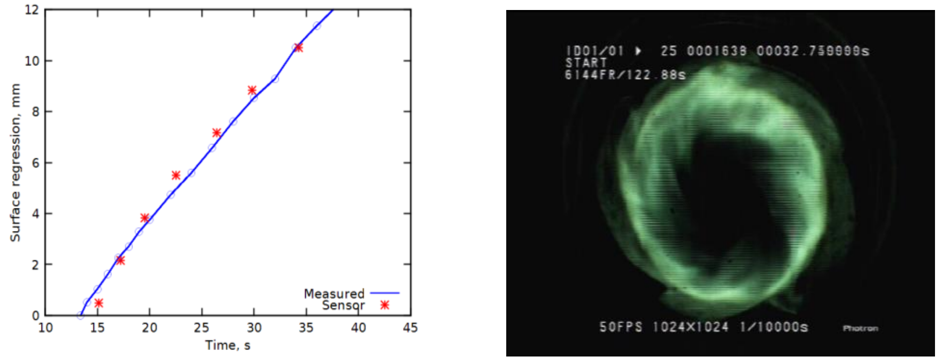

Figure 12: Optical vs. sensor comparison (left) and high-speed combustion visualization (right).

4.1 Post-Processing and Results

The signal transmitted by the sensor appears on the oscilloscope as a series of voltage steps, with a decreasing behavior from the initial voltage level, as shown in Figure 13 (right). A suitable approach to evaluate the regression rate from the sensor signal is the Thickness Over Time (TOT) method [15]. It consists in a finite difference scheme in which the regression rate between two time steps, t_{i+1}-t_i, is calculated as

$$\bar{r}_{f\,i+\frac{1}{2}} = \frac{1}{2}\frac{\bar{D}_{i+1} - \bar{D}_i}{t_{i+1} - t_i} \tag{11}$$

Considering the wire-cut sensor, the distance between wires is known and it represents the difference between the diameter values at the time corresponding to wire break-up. Since the sensor is made by 7 wires, it is possible to obtain 6 measures of the fuel regression rate. The TOT measurement technique, often used in literature, provides easily a discrete set of r_f data with the advantage of not requiring ignition transient analysis. Nevertheless, this method is prone to larger errors. In Figure 13 (left), one can see the calculated TOT regression rate values over the corresponding voltage steps, for a combustion test with HTPB-based fuel and gaseous oxygen as oxidizer. Each TOT discrete value is referred to the average time between two following voltage jumps.

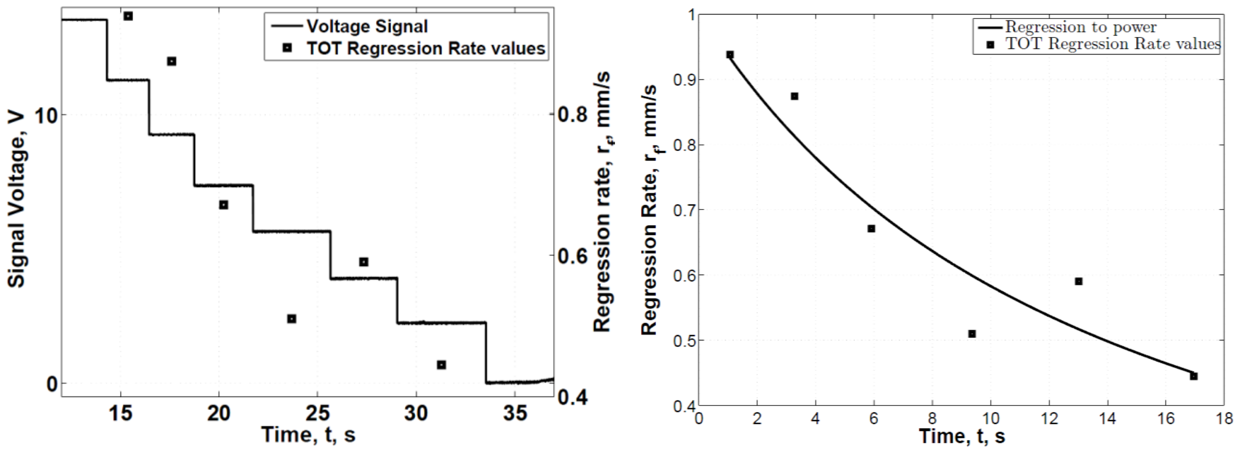

Figure 103: TOT regression rate evaluation (left) and regression rate power law fitting (right).

The TOT values are interpolated by least square method with a power law to obtain an approximate $r_f(t)$, see Figure 13 (right). The origin of the time axis, in Figure 13, corresponds to the instant the first wire breaks at. Similarly, considering the mean diameter between two consecutive wire breaks, $\overline{D}_i$ and $\overline{D}_{i+1}$, it is possible to relate the TOT discrete values with the oxidizer mass flux (corresponding mean diameter), knowing the oxidizer mass flow rate constant value.

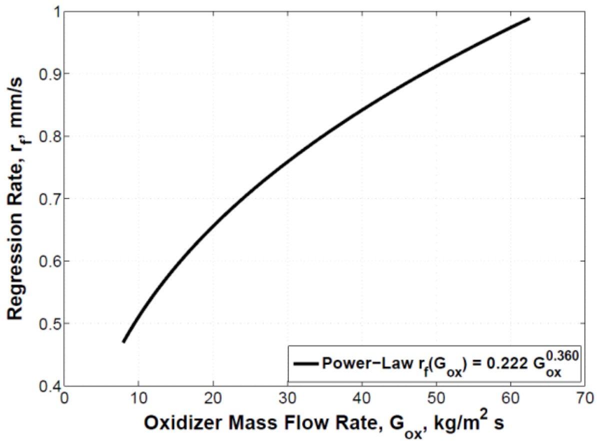

Figure 14: Regression rate vs. oxidizer mass flux.

Then, a standard power-law approximation provides the regression rate as a function of G_{ox}, as shown in Figure 14. However, the sensor provides a local measure of the regression rate in the specific grain location in which it is inserted. Hence, the evaluation of regression rate power-law assumes the same mean diameter on the inner port at the time t_i, without considering the port erosion anisotropy during the combustion. This is not true, because a certain level of anisotropy is always present during the HTPB-based fuel burning. Actually, only few firings with embedded sensor has been performed. Further tests will increase the manufacture accuracy of the sensor. The wire-cut sensor results very suitable to measure the local regression rate inside burner without optical access and for hybrid rocket motors. The use of several sensors carefully distributed in the solid grain can provide a more precise regression rate measure, reducing errors. The combined use of optical video acquisition and wire-cut sensor, inserted in multiple position along the grain length, will allow to obtain a more complete and detailed burning rate characterizations.

5. Conclusions

Three different techniques were developed and currently used in SPLab. The optical time-resolved technique provides a very accurate ballistic characterization sampling the diameter variation with operator-based approach or automatic-based software. The latter has the great advantage to acquire a very high number of measures, giving a better description of the port evolution during the combustion. However, the accuracy of the automatic sampling strongly depends on video filtering operations and requires ad-hoc settings for each combustion video. The current version of the automatic-based software provides correct regression rate trends but the difference with operator-based results is still significant. Hence, improvements of the algorithm and video filtering process are required. Time-resolved technique requires a windowed combustion chamber. This fact represents the main drawback of this approach, involving a more complex experimental setup and higher costs for assembling and maintenance.

Fiber optic sensors have the advantage to be relatively inexpensive, commercially available (communication technology), low interference with combustion process, safety (no electrical discharge/interferences). Although high spatial resolution can be achieved (up to 250 µm), it can be hindered by low fuel opacity.

The wire-cut sensor provides a local measure of the regression surface evolution during the combustion. By using a TOT method, the present version can supply 6 average regression rate values. A wire-cut sensor can be easily embedded in the solid fuel allowing measurements inside combustion chambers without optical access, such as hybrid rocket motors. Moreover, combining the sensor with the optical time-resolved technique, is possible to trigger the video acquisition with sensor signal in order to obtain 7 time intervals, measuring the ignition time of combustion. The combined use of these techniques results also suitable for regression rate measurements at difference distances from the head-end port, in order to investigate the change of fuel burning rate along the sample length. However, the accuracy of wire-cut method is quite lower respect to the time-resolved technique and the measure does not take into account anisotropy combustion effects.

Acknowledgments

The research activity on wire-cut regression rate sensor was supported by SPARTAN (SPAce exploration Research for Throttleable Advanced eNgine), an EC FP7 Space Call Project (GA n. 262837).
The first version of the automatic-based software was developed by C. Galbiati and M. Manzoni in the frame of a technical project (Advanced Propulsion course) at Politecnico di Milano.
The authors are pleased to acknowledge the first theoretical support on fiber optic technology Ing. F. Zoppi (Open Line fiberoptic s.r.l.) and also for fiber optic ribbons procurement.
We would also to thank Ing. P. Tagliabue and N. C. Pistoni (C.E.L.M. – s.n.c. di Campari Enzo) for their support and sharing experience on the first development of the optical set up.

References

[1] DeLuca, L.T, F. Bernelli, F. Maggi, P. Tadini, C. Pardini, L. Anselmo, M. Grassi, D. Pavarin, A. Francesconi, F. Branz, S. Chiesa, N. Viola, V. Trushlyakov, I. Belokonov and C. Bonnal. 2013. Active Space Debris Removal by a Hybrid Propulsion Module. Acta Astronautica, doi: http://dx.doi.org/10.1016/j.actaastro.2013.04.025.

[2] Altman, D. and A. Holzman. 2007. Overview and History of Hybrid Rocket Propulsion. In: Fundamentals of Hybrid Rocket Combustion and Propulsion. Edited by M.J. Chiaverini, and K.K. Kuo, AIAA Progress in Astronautics and Aeronautics, Volume 218, Chapter 1, pp. 1-36.

[3] Chiaverini, M.J. 2007. Review of Solid-Fuel Regression Rate Behavior in Classical and Non classical Hybrid Rocket Motors. In: Fundamentals of Hybrid Rocket Combustion and Propulsion. Edited by M.J. Chiaverini, and K.K. Kuo, AIAA Progress in Astronautics and Aeronautics, Volume 218, Chapter 2, pp. 37-125.

[4] Gibbon, D. M. and G. S. Haag. 2001. Investigation of an alternative geometry hybrid rocket for small orbit transfer. In: Tech. Rep. SPBB-26287-01. Edited by Surrey Satellite Technology Limited.

[5] Annovazzi, A. and L.T. DeLuca. 2009. Solid Rocket Motors. In: Energetic Problems in Aerospace Propulsion, 3rd Edition - Notes for Students. Edited by L.T. DeLuca, Premani, Pantigliate, Milano, Chapter 11, pp. 1-104.

[6] Cauty, F., N. Seryn, and D. Gramer. 2007. Solid-fuel Pyrolysis Phenomena and Regression Rate, Part 2: Measurement Techniques. In: Fundamentals of Hybrid Rocket Combustion and Propulsion. Edited by M.J. Chiaverini, and K.K. Kuo, AIAA Progress in Astronautics and Aeronautics, Volume 218, Chapter 4, pp. 167-205.

[7] Monti, R. and M. Mazzola. 1978. Continuous Regression Rate Measurements in Hybrid Rockets. Experimental Diagnostics in Combustion of Solids, AIAA Progress in Aeronautics and Astronautics, Edited by T.L. Boggs and B.T. Zinn, Vol. 63, pp. 111-128.

[8] Waterfall, R.C., R. He, P. Wolanski, and Z. Gut. 1999. Monitoring Flame Position and Stability in Combustion Cans Using ECT. Presented at 1st World Congress on Industrial Process Tomography, Buxton, Greater Manchester.

[9] Carmicino, C., G. Giulietti, T. Marchione, F. Lavorgna, and A.M. Russo Sorge. 2003. Regression Rate Measurements in a Hybrid Rocket. In: Volume 8 of IWCP (International Workshop on Chemical Propulsion) - Rocket Propulsion: Present and Future. Edited by L.T. DeLuca, Grafiche CSS Bergamo, Italy, Paper number: IWCP-08-13.

[10] Marxman, G.A. and M. Gilbert. 1963. Turbulent Boundary Layer Combustion in the Hybrid Rocket. In: 9th International Symposium on Combustion, Academic Press, Inc., New York, pp. 371-383.

[11] Houser, T.J. and M.V. Peck. 1964. Research in Hybrid Combustion. In: Vol. 15 of AIAA Progress in Astronautics and Aeronautics, Heterogeneous Combustion, Edited by H.G. Wolfhard, I. Glassman, and L. Green Jr. Academic Press, New York, NY, USA, pp. 559-581.

[12] DeZilwa, G. Ziliac, M. Reinat, and M.A. Karabeyoglu. 2004. Time-Resolved Fuel-Grain Port Diameter Measurement in Hybrid Rockets. Journal of Propulsion and Power, Vol. 20, No. 4, pp. 684-689.

[13] Evans, B., G.A. Risha, N.A. Favorito, E. Boyer, R.B. Wehrman, N. Libis, and K.K. Kuo. 2003. Instantaneous Regression Rate Determination in a Cylindrical X-ray Transparent Hybrid Rocket Motor. AIAA Paper 03-4592.

[14] Evans, B., E. Boyer, K.K. Kuo, G. Risha, and M.J. Chiaverini. 2009. Hybrid Rocket Investigations at Penn State University's High Pressure Combustion Laboratory: Overview and Recent Results. AIAA Paper 2009-5349.

[15] DeLuca, L.T., L. Galfetti, F. Maggi, G. Colombo, L. Merotto, M. Boiocchi, C. Paravan, A. Reina, P. Tadini, and L. Fanton. 2012. Characterization of HTPB-based Solid Fuel Formulations: Performance, Mechanical Properties, and Pollution. Acta Astronautica, doi: http://dx.doi.org/10.1016/j.actaastro.2012.05.002.

[16] DeLuca, L.T., L. Galfetti, G. Colombo, F. Maggi, A. Bandera, M. Boiocchi, G. Gariani, L. Merotto, C. Paravan, and A. Reina. 2011. Time–Resolved Burning of Solid Fuels for Hybrid Rocket Propulsion. In: *Advances in Propulsion Physics, Vol. 2,* Edited by: L.T. DeLuca, C. Bonnal, O. Haidn and S.M. Frolov, Torus Press, Moscow, 341–362.
[17] Paravan, C., A. Reina, A. Sossi, M. Manzoni, G. Massini, G. Rambaldi, E. Duranti, A. Adami, E. Seletti and L. T. DeLuca. 2012. Time-resolved Regression Rate of Innovative Solid Fuel Formulations. In: *Progress in Propulsion Physics, Vol.* 4, Edited by: L.T. DeLuca, C. Bonnal, O. Haidn and S.M. Frolov, Torus Press, Moscow, 75-98.
[18] Paravan, C. 2012. Ballistics of Innovative Solid Fuel Formulations for Hybrid Rocket Engines. PhD Dissertation, Politecnico di Milano, Dept. of Aerospace Sciences and Technologies.
[19] Ohlemiller, T.J. and M. Summerfield. 1968. A Critical Analysis of Arc Image Ignition of Solid Propellants. AIAA Journal, Vol.6, No.5, pp. 878-886.
[20] Incropera, F.P. and D.P. DeWitt. 1990. Fundamentals of Heat and Mass Transfer, 3rd Edition. Wiley, New York, p. 515.
[21] Fanton, L., C. Paravan, and L.T. DeLuca. 2012. Testing and Modeling Fuel Regression Rate in a Miniature Hybrid Burner. International Journal of Aerospace Engineering.
[22] Evans, B., N. A. Favorito, E. Boyer, and K.K. Kuo. 2004. Characterization of Solid Fuel Burning Rates in an X-Ray Transparent Hybrid Rocket Engine. AIAA Paper 2004-3821.
[23] Benterou, J., Udd, E. 2007. Measurements Using Fiber-optic Bragg Grating Sensors. EuroPyro, 34th International Pyrotechnics Seminar, Beaune, France.
[24] Udd, E., Benterou, J. 2010. Review of High-Speed Fiber Optic Grating Sensors Systems. SPIE Defense, Security and Sensing, 7677-Fiber Optic sensors and Applications VII, Orlando, United States.
[25] Beer, J.M., and N.A. Chigier. 1972. Combustion Aerodynamics. Applied Science.